Formation of Stable Ag-Nanoparticle Aggregates Induced by Dithiol Cross-Linking

Päivi Ahonen,[†] Timo Laaksonen,[†] Antti Nykänen,[‡] Janne Ruokolainen,[‡] and Kyösti Kontturi*[,†]

Laboratory of Physical Chemistry and Electrochemistry, Helsinki University of Technology, P.O. Box 6100, FIN-02015 HUT, Finland, and Department of Engineering Physics and Mathematics and Center of New Materials, Helsinki University of Technology, P.O. Box 2200, FI-02015 HUT, Espoo, Finland

Received: January 23, 2006; In Final Form: May 15, 2006

Aggregation of thiol-stabilized silver nanoparticles induced by 1,6-hexane dithiol was studied in situ by dynamic light scattering. The aggregates were observed to reach a finite size in the 100−200 nm range depending on the applied conditions. Growth kinetics were shown to be linked to the dynamics of the thiol-exchange reaction. A model for the aggregation process was developed on the basis of a simple diffusion-kinetic approach assuming an elementary kinetic reaction at the surfaces and a spherical diffusion field surrounding the aggregates. The rate constant for the thiol exchange reaction was found to vary between 0.6 and 4.0 × 10^{-4} s^{-1}, and the activation energy was 46 ± 10 kJ mol^{-1}.

Introduction

During the past decade, a significant amount of work has been carried out in the field of functionalized monolayer-protected clusters (MPCs). The pioneering work of Brust et al. in the synthesis of alkanethiolate-protected[1] and functionalized[2] nanoparticles was followed by the introduction of place-exchange reactions with other thiol ligands by Murray et al.[3,4] Place-exchange reactions can be used to form self-assembled nanoparticle structures by cross-linking particles with α,ω-functionalized ligands.[5] Materials formed in this way maintain many of the unusual properties of their original nanosized components because the MPCs remain segregated.[6,7] The properties are also tunable because the distance separating the particles is well defined by the choice of dithiol. Thus far, the dynamics for the formation of superstructures of the kind described here has received very little attention as studies of place-exchange have focused on individual MPCs. Several reports of both noncovalent-[8,9] and dithiol-induced[10−18] self-assembly of nanoparticles have surfaced. They consider mostly electrical and optical properties of the nanoparticle materials formed, instead of the kinetics of the aggregation process addressed in this work. Some studies on smaller, more defined, nanoparticle structures[19−21] have also been published.

Dynamic light scattering (DLS) is a convenient way to measure size changes of nanoparticles and their colloidal aggregates in situ. In other techniques such as SEM and TEM, samples must be taken and the reaction quenched at appropriate time intervals. With DLS, one can follow the evolution of colloid size in the same sample without the tedious work required to prepare one sample for each time step. While DLS is limited to following the hydrodynamic radius and cannot give the actual geometry of the measured object, the method is satisfactory for characterizing and monitoring changes in well-defined colloidal systems. DLS has already been used to follow various kinds of aggregation processes. For further information, a recent review from Sandkühler et al.[22] and references therein are recommended. Recently, commercial instruments based on backscattering have become available. Collecting the backscattered light avoids multiple scattering from the particles and facilitates the measurement of strongly absorbing colloids. These instruments can characterize sizes even smaller than 2 nm.[23,24]

While the thiol exchange of dithiols cannot be directly observed with DLS, aggregation caused by cross-linking of nanoparticles can easily be monitored. It is common to use a power law to describe the aggregate growth,[25] but this gives very little quantitative information. Instead, we have applied a simple theoretical model, which links the aggregation rate to the rate of the thiol exchange reaction. This way, it is possible to probe the thiol exchange reaction indirectly by following the aggregation kinetics.

Experimental Section

Chemicals. Silver nitrate ($AgNO_3$, Premion, Alfa Aesar), tetraoctylammonium bromide (TOABr, 98 +%, Alfa Aesar), sodium borohydride ($NaBH_4$, Merck), 1-dodecane thiol (98%, Lancaster), and 1,6-hexane dithiol (97%, Lancaster) were used as received. Toluene (p.a., Riedel de Haën) and acetone (p.a. Fluka) were used without further purification.

Synthesis of Monolayer-Protected Silver Nanoparticles. The synthesis of silver nanoparticles was performed by a two-phase method adapted from the literature.[1] In the first part of the synthesis, 3 mmol of silver nitrate was dissolved in 200 mL of Milli-Q water. Silver ions were then transferred into the organic phase with aid of *n*-tetraoctylammonium bromide as the phase-transfer reagent. The organic phase was 300 mL of toluene. The completeness of the phase transfer was ascertained by using an excess of TOABr (9 mmol). The phases were separated after 3 h of stirring, and dodecane thiol was added into the organic phase, which was then stirred for about 15 min. The dodecanethiol-to-silver ratio was 5:3. Sodium borohydride was used as the reducing agent. A 10-fold excess of sodium borohydride in 150 mL of aqueous solution was added dropwise into the reaction flask. The reaction was allowed to proceed for 2 h. After reduction, the solvent was removed with a rotary evaporator. The nanoparticles were precipitated with acetone at reduced temperature, −18 °C. The toluene-soluble particles

* Corresponding author. E-mail: kontturi@cc.hut.fi.
[†] Laboratory of Physical Chemistry and Electrochemistry.
[‡] Department of Engineering Physics and Mathematics and Center of New Materials.

10.1021/jp0604692 CCC: $33.50
Published on Web 06/10/2006

were washed with acetone and separated by centrifugation. The washing process was repeated three times. The silver nanoparticle solutions were protected from light during the whole synthesis.

Dynamic Light Scattering. The measurements of the size evolution of the nanoparticle aggregates were performed with a Zetasizer Nano ZS (Malvern Instruments). A 4 mW 633 nm He−Ne laser was used as the light source, and the scattered light was measured at 173° to prevent multiple scattering. The data were analyzed using standard procedures in the software provided with the instrument. The measurements were carried out in glass cuvettes using 0.44 mg/mL toluene solutions of nanoparticles. 1,6-Hexane dithiol was used as the linker molecule, and it was added so that its concentration in different samples was 0.08, 0.40, and 0.80 mM. The MPC concentration was kept constant in all measurements. The measurements were repeated at three temperatures, 10, 25, and 40 °C, to gain information on the kinetics of the nucleation and growth of the silver MPC aggregates. No stirring was used during the measurement to keep the growth reaction under diffusion control. If the solution was stirred vigorously during the measurement, rapid aggregation was observed. The dithiols were added rapidly into the solution to get a homogeneous initial concentration. For better reproducibility, a fixed volume of dithiol solution was used in every experiment with no subsequent stirring. The nanoparticle aggregates obtained via this reaction were remarkably stable and did not precipitate or grow over periods of more than 24 h after reaching their limiting size.

Because the instrument measures size by first evaluating mobility, that is, diffusion coefficient, additional information about the diffusion of aggregates of different sizes was obtained simultaneously from the same measurements.

Transmission Electron Microscopy (TEM). The initial nanoparticle size distribution was confirmed with TEM. The measurements were performed on a Tecnai 12 instrument operating at a 120 kV accelerating voltage. The samples were prepared by placing a drop of nanoparticles in a toluene solution on Formvar/carbon-coated copper grids (Electron Microscopy Sciences). The grids were dried in air. Size analysis was made using the ImageJ software.

Cryo-TEM was done to get information about the 3D-structure of the aggregates, specifically whether they are very fractal in nature or denser, closely packed clusters. The target of the cryo-TEM sample preparation was to achieve vitrified amorphous electron-visible thin films of the toluene solution by rapidly freezing it. Using this method, it is possible to preserve the solution-state structure. First, 6 μL of sample solution was applied on a Quantifoil R2/2 holey carbon film coated copper grid and blotted for 1−2 s with Macherey-Nagel MN640w filter paper. Immediately after blotting, the grid was plunged in liquid nitrogen using a guillotine apparatus made for this purpose. Liquid nitrogen was used instead of more rapidly freezing liquid ethane to prevent toluene thin film from etching. After quenching, the grid was kept at liquid nitrogen temperature and transferred to TEM by using a Gatan 910 cryotransfer-holder. Bright field imaging was performed on the same instrument as above.

Theoretical Calculations

Kinetic Model for Aggregate Growth. A model based on a simple diffusion-kinetic scheme was devised to get kinetic information about the thiol exchange reaction.[26,27] A monomer-aggregate growth mechanism was assumed to gain a mathematically simple model. In this study, monomers refer to MPCs that have dithiols place-exchanged onto their surface. Aggregates refer to assemblies of nanoparticles linked by dithiols. In the model, dithiol-functionalized particles are assumed to be monomers, which are attaching and detaching from growing aggregates. It is reasonable to assume that nonfunctionalized particles will not attach to the aggregates to the same extent as functionalized particles as they are less reactive. This assumption is supported by the experimental results presented later on. Growth by combination of aggregates is also neglected in the model based on the slowness of their diffusion and comparably low concentration. This assumption is supported by the observed extensive long-term aggregate stability and their limiting size. Furthermore, all aggregates are assumed to be spherical and of the same size. While there certainly will be a distribution in size, this assumption simplifies the model greatly and reduces the number of parameters required. The reaction scheme is illustrated in Scheme 1. A fixed number of nucleation points are assumed to exist throughout the experiment.

SCHEME 1: Schematic Reaction Mechanism for Cluster Growth[a]

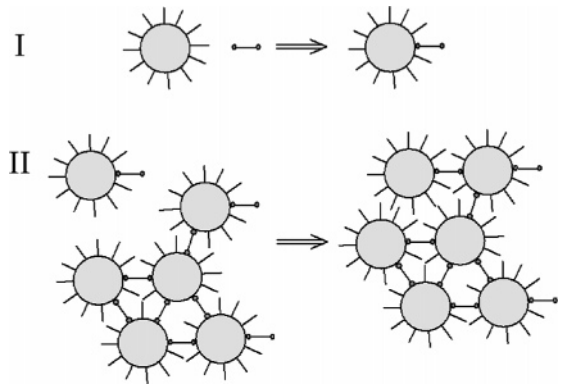

[a] In phase I, functionalized monomers are formed, and in phase II monomers attach to an aggregate.

The supply of monomers is dictated by the ligand-exchange reaction as follows:

$$\text{nanoparticle} + \text{dithiol} \rightarrow \text{functionalized nanoparticle} \quad (1)$$

The monomer mass balance is thus given by the difference in the monomer formation rate and the incorporation of monomers in the aggregates.

$$\frac{dc_{M,bulk}}{dt} = k_e c_{NP}{}^{u} c_{DT}{}^{v} - \frac{c_{Nucl}}{V_m}\frac{dV}{dt} \quad (2)$$

where $c_{M,bulk}$, c_{NP}, and c_{DT} are the bulk concentration of the monomer, concentration of the nanoparticles, and concentration of dithiol, respectively, k_e is the rate constant for thiol exchange, $n = u + v$ is the order of the reaction, r is the mean radius of the aggregates, V_m is the volume of the monomer, V is the volume of the aggregate, and c_{Nucl} is the concentration of nucleation sites.

Next, we define the growth flux J_g and the flux of monomer desorption from the aggregates J_d:

$$J_g = 4\pi r^2 k_a c_{M,r} \quad (3)$$

$$J_d = 4\pi r^2 k_d \quad (4)$$

where k_a is the rate constant for attaching a monomer, k_d is the

rate constant for desorption of the monomer, and $c_{M,r}$ is the concentration of the monomer close to the surface of the cluster. Furthermore, the equilibrium constant, K_{eq}, is defined as the ratio between rate constants for detachment and attachment:

$$K_{eq} = \frac{k_d}{k_a} \tag{5}$$

K_{eq} is assumed to be very low, because monomers in the aggregate are tightly bound through multiple dithiol bonds. The diffusion flux toward the surface of the aggregate must equal the growth rate and is obtained from Fick's first law in spherical coordinates, assuming that the moving boundary due to growth can be neglected.[28] This assumption is valid for the slow growth considered here. Hence, monomer's diffusion flux near the aggregate's surface is given by:

$$J_{diff} = 4\pi Dr(c_{M,bulk} - c_{M,r}) \tag{6}$$

where D is the diffusion coefficient of nanoparticles.

In the stationary state, the flux balance dictates that attachment and detachment fluxes are equal to the diffusion flux:

$$J_g - J_d = J_{diff} \tag{7}$$

Combining eqs 3−7 gives us the monomer concentration near the surface of the aggregate:

$$c_{M,r} = \frac{Dc_{M,bulk} + rk_d}{rk_a + D} \tag{8}$$

The volume change of the aggregate can be obtained from the diffusion flux, which is in effect the accumulation flux:

$$N_a V_m J_{diff} = \frac{dV}{dt} \tag{9}$$

where N_a is Avogadro's number.

Combining eqs 6, 8, and 9 gives:

$$\frac{dr}{dt} = N_a V_m D\left(\frac{c_{M,bulk} - K_{eq}}{r + D/k_a}\right) \tag{10}$$

Thus, we can rewrite eq 2 in the following form:

$$\frac{dc_{M,bulk}}{dt} = k_e c_{NP}{}^u c_{DT}{}^v - 4\pi r^2 N_a D c_{Nucl} \frac{c_{M,bulk} - K_{eq}}{r + D/k_a} \tag{11}$$

Furthermore, in the calculations we also have to take into account the mass balance of all other species.

Results and Discussion

The size of the nanoparticles' metal core was determined from TEM-micrographs and was 2.9 ± 0.8 nm. In comparison, the hydrodynamic radius of the nanoparticles measured by light scattering was 5.3 nm. The hydrodynamic radius of the particle includes the dodecane thiols as well as trapped solvent molecules. The thickness of the thiol and the trapped solvent layer, 1.2 nm, is slightly smaller than the length of a dodecanethiol molecule, 1.5 nm,[29] probably due to the free-draining of the dodecanethiols' end groups.[30] The size of the silver core corresponds to a stable geometry of a truncated octahedron consisting of 314 atoms[31] and ca. 90 ligands,[32] from which an approximate molar mass was calculated. Based on this, the molar concentration of the MPCs in every sample was 0.085 mM; thus the ratios of dithiol to MPCs were 9, 47, and 97 corresponding to 0.08, 0.4, and 0.8 mM dithiol concentrations.

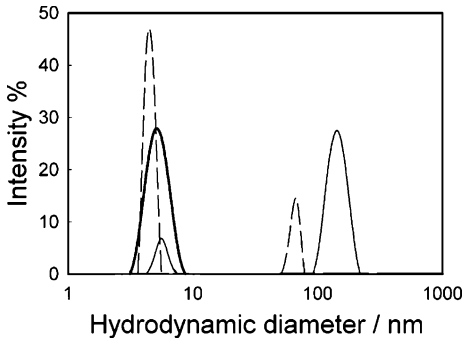

Figure 1. Intensity distribution of aggregate hydrodynamic diameters before (bold line), after 5 min (dashed line), and after 35 min (solid line) of the addition of dithiol. Equivalent amounts of MPCs and dithiol were used in the experiment. Logarithmic scale is used for the hydrodynamic diameter.

In all of the measurements, a rapid growth stage followed by leveling out of the hydrodynamic radius was observed. Finally, a stable size was reached when the solution was depleted of nanoparticles. This was ascertained by the absence of free nanoparticles in the cryo-TEM micrographs. The final hydrodynamic radius was between 100 and 160 nm in all of the measurements. This size did not change noticeably even after 24 h, indicating that aggregates do not have the tendency to combine in the time-scale considered.

The assumption of the cluster-particle growth was drawn from the difference between the mobilities of a single nanoparticle and an aggregate. The measured diffusion coefficient for a nanoparticle, 1.4×10^{-6} cm^2 s^{-1}, is significantly higher than that measured for the aggregates, 5.0×10^{-8} cm^2 s^{-1}, which supports the above assumption. It is also assumed that the reaction between a nanoparticle and a free dithiol cannot be slower than that between a nanoparticle and the free end of a dithiol that has already been attached to another particle.

Evidence of the monomer growth mechanism was obtained when equivalent amounts of dithiol and MPCs were used (Figure 1.). Before the addition of the dithiol, only one peak near 5 nm corresponding to nanoparticles is shown in the intensity distribution. Five minutes after the addition, a second peak at 65 nm appears, but the initial peak remains the most intensive. As the growth of the larger clusters continues further, the second peak moves toward larger sizes and the first peak remains at the initial size, losing its intensity. It is pointed out here that the scattering efficiency of large objects is much larger than that of small ones, which, considering the monomer/aggregate peak intensity, means that the concentration of the growing aggregates is very low as compared to free particles. The absence of small clusters >5 nm in size is a good indication for the monomer-cluster growth mechanism.

Cryo-TEM images showed that the aggregates were quite densely packed as shown in Figure 2. This also corroborates the assumed monomer-cluster growth mechanism, which should yield more condensed aggregates than the aggregate−aggregate mechanism.[33] The nanoparticles were very close to each other in the aggregates as was expected due to the short linker molecule, but had not changed in size. Also, very few free nanoparticles were observed, indicating that almost all of them had been consumed by the aggregates.

The kinetic model was fitted manually to experimental data (Figure 3a−c). The number of nucleation points was kept as

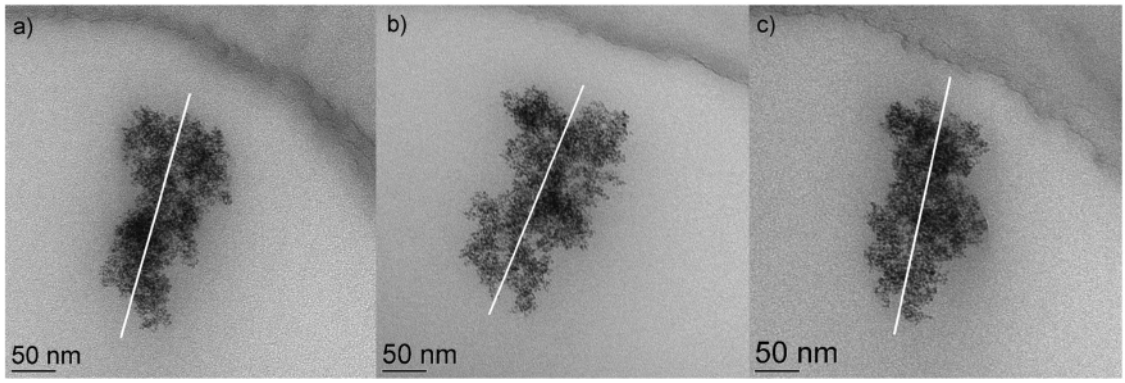

Figure 2. Cryo-TEM images of an Ag nanoparticle aggregate tilted at −50° (a), 0° (b), and 50° (c). The white line corresponds to the approximate center line of the aggregate at different tilt angles.

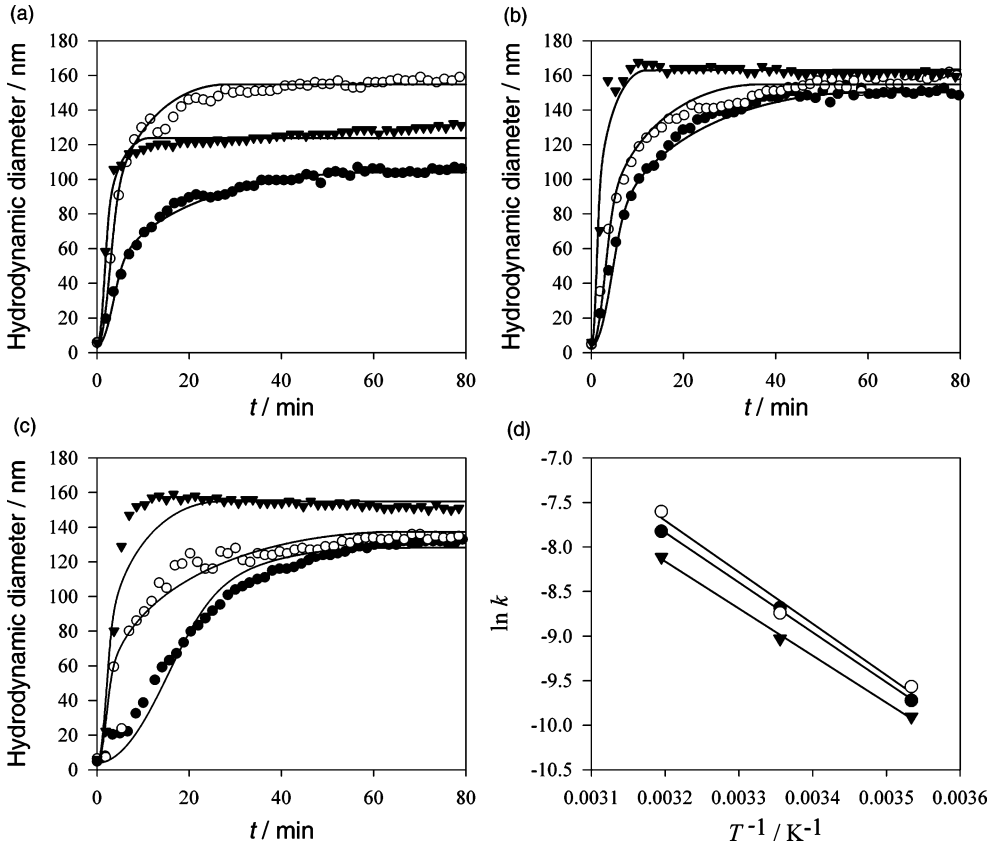

Figure 3. Evolution of the hydrodynamic radius of the nanoparticle aggregate: experimental results (dots) and calculated values (solid lines). Concentration parameter *S* was 94 (a), 47 (b), and 9 (c). Temperature was set to 10 °C (●), 25 °C (○), and 40 °C (▼). Arrhenius plot (d) is shown for the same calculations. *S* was 94 (▼), 47 (○), and 9 (●).

TABLE 1: Thiol Exchange Rate Constants and Concentrations of Nucleation Points[a]

temperature	k_e/s^{-1} $S = 94$	k_e/s^{-1} $S = 47$	k_e/s^{-1} $S = 9$	c_{Nucl}/M $S = 94$	c_{Nucl}/M $S = 47$	c_{Nucl}/M $S = 9$
10 °C	0.6×10^{-4}	0.8×10^{-4}	0.7×10^{-4}	23×10^{-8}	8.2×10^{-8}	3.5×10^{-8}
25 °C	1.2×10^{-4}	1.3×10^{-4}	1.6×10^{-4}	7.7×10^{-8}	7.8×10^{-8}	11×10^{-8}
40 °C	3.0×10^{-4}	4.0×10^{-4}	4.0×10^{-4}	15×10^{-8}	6.4×10^{-8}	7.5×10^{-8}

[a] *S* is the concentration parameter describing the amount of supersaturation, that is, the dithiol to MPC ratio.

an empirical value, which was fitted separately for all measurements. It is virtually impossible to accurately control the number of nucleation points in practice due to the difficulty of reproducing the injection of dithiol into the solution. Thus, some variation in the number of aggregates was always seen. It was found that the values of K_{eq} and k_a were small and played only a minor role in the shape of the calculated curve, and could not therefore be conclusively fitted. The number of nucleation points dictated the final size of the cluster, and k_e determined the shape of the curve. Therefore, these two could be fitted quite well. The values of k_e were further used to calculate the value of the activation energy from the standard $\ln k = \ln k_0 + \Delta G_{act}/RT$ plot (Figure 2d). The measurement data conform best to pseudo first-order reaction kinetics where $n = 1$ and $u = v = 0.5$, because then the concentration dependence of the Arrhenius plot vanishes almost completely. This yields a value of 46 ± 10 kJ

mol^{-1} for the activation energy of reaction 1. For second-order kinetics, the same value for activation energy was obtained, but the values of k_0 were concentration dependent. Values of k_e and c_{Nucl} used in the calculations are listed in Table 1.

Values of the pseudo-first-order kinetic constants were found to vary between 0.6 and 4.0 $\times$ 10^{-4} s^{-1} depending on the temperature. Because there are no reported data about the kinetics of thiol-exchange on silver nanoparticles, they can only be compared with studies done on gold nanoparticles. Here, measured values correspond rather well with those obtained by Donkers et al.[34] for ligand-exchange of substituted arylthiolates on gold nanoparticles. Because of their better stability, dodecanethiol-protected silver nanoparticles were used, instead of hexanethiol-stabilized. The hexanedithiol linker being much shorter than the capping layers, there is presumably some steric hindrance slowing down the reaction. Thus, the place-exchange of thiols on silver nanoparticles seems to be faster than on gold nanoparticles.

Conclusions

Formation of stable clusters of nanoparticles could be obtained by chemically bonding silver nanoparticles together with hexanedithiol. The evolution of aggregate size could be readily monitored via dynamic light scattering. Stable aggregates of around 140 nm were reproducibly obtained if the reaction was allowed to be under diffusion control. No further increase in aggregate size was observed after an initial growth period of about 60 min. Kinetic information about the thiol exchange reaction could be obtained with a simple model where the reaction is considered to proceed with dithiol-functionalized nanoparticles attaching to a growing nanoparticle cluster. The activation energy for the ligand-exchange reaction was calculated to be 46 $\pm$ 10 kJ mol^{-1}. In summary, we have demonstrated that dynamic light scattering provides a simple and effective means of probing the kinetics of place-exchange reactions on nanoparticle surfaces.

Acknowledgment. This research was supported by a grant from the Kemira Foundation. We thank Dr. Christoffer Johans and Dr. Bernadette Quinn for their helpful comments during the study and preparation of this manuscript.

References and Notes

(1) Brust, M.; Walker, M.; Bethell, D.; Schiffrin, D. J.; Whyman, R. *J. Chem. Soc., Chem. Commun.* **1994**, 801.

(2) Brust, M.; Fink, J.; Bethell, D.; Schiffrin, D J.; Kiely, C. *J. Chem. Soc., Chem. Commun.* **1995**, 1655.

(3) Hostetler, M. J.; Green, S. J.; Stokes, J. J.; Murray, R. W. *J. Am. Chem. Soc.* **1996**, *118*, 4212.

(4) Hostetler, M. J.; Templeton, A. C.; Murray, R. W. *Langmuir* **1999**, *15*, 3782.

(5) Brust, M.; Bethell, D.; Schiffrin, D. J.; Kiely, C. J. *Adv. Mater.* **1995**, *7*, 795.

(6) Brust, M.; Bethell, D.; Kiely, C. J.; Schiffrin, D. J. *Langmuir* **1998**, *14*, 5425.

(7) Gittins, D. I.; Bethell, D.; Nichols, R. J.; Schiffrin, D. J. *Adv. Mater.* **1999**, *11*, 797.

(8) Fullam, S.; Rao, S. N.; Fitzmaurice, D. *J. Phys. Chem. B* **2000**, *104*, 6164.

(9) Ryan D.; Rao, S. N.; Rensmo, H.; Fitzmaurice, D.; Preece, J. A.; Wenger, S.; Stoddart, J. F.; Zaccheroni, N. *J. Am. Chem. Soc.* **2000**, *122*, 6252.

(10) Bethell, D.; Brust, M.; Schiffrin, D. J.; Kiely, C. *J. Electroanal. Chem.* **1996**, *409*, 137.

(11) McConnell, W. P.; Novak, J. P.; Brousseau, L. C., III; Fuirerer, R. R.; Tenent, R. C.; Feldheim, D. L. *J. Phys. Chem. B* **2000**, *104*, 8925.

(12) Mayer, C. R.; Neveu, S.; Cabuil, V. *Adv. Mater.* **2002**, *14*, 595.

(13) Kulkarni, G. U.; Thomas, P. J.; Rao, C. N. R. *Pure Appl. Chem.* **2002**, *74*, 1581.

(14) Torma, V.; Vidoni, O.; Simon, U.; Schmid, G. *Eur. J. Inorg. Chem.* **2003**, 1121.

(15) Zhong, Z.; Patskovskyy, S.; Bouvrette, P.; Luong, J. H. T.; Gedanken, A. *J. Phys. Chem. B* **2004**, *108*, 4046.

(16) Wessels, J. M.; Nothofer, H.-G.; Ford, W. E.; von Wrochem, F.; Scholz, F.; Vossmeyer, T.; Schroedter, A.; Weller, H.; Yasuda, A. *J. Am. Chem. Soc.* **2004**, *126*, 3349.

(17) Huang, W.; Masuda, G.; Maeda, S.; Tanaka, H.; Ogawa, T. *Chem.-Eur. J.* **2005**, *12*, 607.

(18) Guarise, C.; Pasquato, L.; Scrimin, P. *Langmuir* **2005**, *21*, 5537.

(19) Haiss, W.; Nichols, R. J.; Higgins, S. J.; Bethell, D.; Höbenreich, H.; Schiffrin, D. J. *Faraday Discuss.* **2004**, *125*, 179.

(20) Novak, J. P.; Feldheim, D. L. *J. Am. Chem. Soc.* **2000**, *122*, 3979.

(21) Shibu Joseph, S. T.; Ipe, B. I.; Pramod, P.; Thomas, K. G. *J. Phys. Chem. B* **2006**, *110*, 150.

(22) Sandkühler, P.; Lattuada, M.; Wu, H.; Sefcik, J.; Morbidelli, M. *Adv. Colloid Interface Sci.* **2005**, *113*, 65.

(23) D'Souza, L.; Suchopar, A.; Richards, R. M. *J. Colloid Interface Sci.* **2004**, *279*, 458.

(24) Pecora, R. *J. Nanopart. Res.* **2000**, *2*, 123.

(25) Weitz, D. A.; Huang, J. S.; Lin, M. Y.; Sung, J. *Phys. Rev. Lett.* **1985**, *54*, 1416.

(26) Talapin, D. V.; Rogach, A. L.; Haase, M.; Weller, H. *J. Phys. Chem.* **2001**, *105*, 12278.

(27) Voyutsky, S. *Colloid Chemistry*; Mir Publishers: Moscow, 1975.

(28) Zener, C. *J. Appl. Phys.* **1949**, *20*, 950.

(29) Wuelfing, W. P.; Green, S. J.; Pietron, J. J.; Cliffel, D. E.; Murray, R. W. *J. Am. Chem. Soc.* **2000**, *122*, 11465.

(30) Wuelfing, W. P.; Templeton, A. C.; Hicks, J. F.; Murray, R. W. *Anal. Chem.* **1999**, *71*, 4069.

(31) Whetten, L.; Khoury, J. T.; Alvarez, M. M.; Murthy, S.; Vezmar, I.; Wang, Z. L.; Stephens, P. W.; Cleveland, C. L.; Luedtke, W. D.; Landman, U. *Adv. Mater.* **1996**, *8*, 428.

(32) Hostetler, M. J.; Wingate, J. E.; Zhong, C.-J.; Harris, J. E.; Vachet, R. W.; Clark, M. R.; Londono, J. D.; Green, S. J.; Stokes, J. J.; Wignall, G. D.; Glish, G. L.; Porter, M. D.; Evans, N. D.; Murray, R. W. *Langmuir* **1998**, *14*, 30.

(33) Brinker, C. J.; Scherer, G. W. *Sol−Gel Science: The Physics and Chemistry of Sol−Gel Processing*; Academic Press: San Diego, 1990.

(34) Donkers, R. L.; Song, Y.; Murray, R. W. *Langmuir* **2004**, *20*, 4703.